

# Model reconstructions for the Si(337) orientation

Feng-Chuan Chuang

Ames Laboratory – US Department of Energy, and  
Department of Physics, Iowa State University, Ames, IA 50011, USA

Cristian V. Ciobanu\*

Division of Engineering, Colorado School of Mines, Golden, CO 80401, USA

Cai-Zhuang Wang and Kai-Ming Ho

Ames Laboratory – US Department of Energy, and  
Department of Physics, Iowa State University, Ames, IA 50011, USA

September 11, 2018

## Abstract

Although unstable, the Si(337) orientation has been known to appear in diverse experimental situations such as the nanoscale faceting of Si(112), or in the case of miscutting a Si(113) surface. Various models for Si(337) have been proposed over time, which motivates a comprehensive study of the structure of this orientation. Such a study is undertaken in this article, where we report the results of a genetic algorithm optimization of the Si(337)-(2 × 1) surface. The algorithm is coupled with a highly optimized empirical potential for silicon, which is used as an efficient way to build a set of possible Si(337) models; these structures are subsequently relaxed at the level of ab initio density functional methods. Using this procedure, we retrieve the (337) reconstructions proposed in previous works, as well as a number of different ones.

---

\*Corresponding author, email: cciobanu@mines.edu

# 1 Introduction

Silicon surfaces have been at the foundation of the semiconductor industry for several decades. With the advent of nanotechnology, the interest in the atomic structure of various semiconductor surfaces has expanded because of their potential to serve as natural and inexpensive templates for growing various types of nanostructures. Understanding the growth of nanoscale entities on various substrates depends, at least in part, on knowing the atomic structure of the substrate. As the low-index crystal surfaces are well understood, the high-index orientations are now progressively gaining importance as their richer morphological features may lead to more advanced technological applications. To date, there are numerous stable high-index orientations reported in the literature; in the case of Silicon and Germanium, these stable orientations have been summarized in Ref. [1]. The *unstable* high-index orientations are important in their own right, as they often give rise to remarkable periodic grooved morphologies which may be used for the growth of surface nanowires. The wonderful morphological and structural diversity of high-index surfaces can be appreciated, for instance, from the work of Baski, Erwin and Whitman, who investigated systematically the surface orientations between Si(001) and Si(111) [2].

An interesting case of unstable surface is Si(337), whose atomic structure is the subject of the present article. As a historical account, we note that the Si(337) orientation was concluded to be stable in early studies by Ranke and Xing [3], Gardeniers *et al.* [4], and Hu *et al.* [5]. This conclusion about the stability of Si(337) was consistent with the reports of Baski and Whitman, who showed that Si(112) decomposes into quasi-periodic Si(337) and Si(111) nanofacets [6], and that Si(337) is a low-energy orientation [7]. However, further studies by Baski and Whitman revealed that Si(337) itself facets into Si(5 5 12) and Si(111) [8], demonstrating that Si(337) was, in fact, unstable. Since Si(337) is not stable and Si(5 5 12) is [9, 10], the clean Si(112) orientation should facet into Si(5 5 12) and Si(111). However, as explained in Ref. [8], nanofacets are too narrow

to form complete Si(5 5 12) units, and mostly settle for the nearby Si(337) orientation. A more recent report [11] shows another situation where Si(337) arises rather than the expected Si(5 5 12). For a Si(113) surface that is miscut towards [111], the large (5 5 12) reconstruction has not always been found. Instead, a Si(337) phase has been seen to coexist with Si(113) terraces [11]. The high resolution transmission electron microscope (HRTEM) images in Ref. [11] leave no doubt that the periodicity of those nanofacets corresponds to the (337) orientation. The reason for the quasi-stability of Si(337) reported in earlier works [3, 4, 5] could be the curvature or the size of substrates used in those investigations; this explanation is also consistent with Ref. [11], where the issue of sample curvature is acknowledged.

With one exception [5], atomic-scale models for Si(337) were not sought separately, but rather as structural parts of the Si(5 5 12)-(2 × 1) reconstruction [9, 12, 13, 14]. As shown in Ref. [9], the Si(5 5 12) unit cell consists of two Si(337) units and one Si(225) unit. The first model reconstruction proposed for Si(5 5 12) [9] appeared somewhat corrugated when viewed along the  $\bar{1}10$  direction; so did a second model by Ranke and Xing [12]. On the other hand, HRTEM measurements [13] showed a flatter profile for Si(5 5 12), and different model reconstructions were proposed [13, 14] in order to account for the observed flatness. Total-energy density functional calculations for the energy of Si(5 5 12) have only recently been published, and suggest that the latest models [13, 14] have lower energies than the earlier proposals [9, 12].

The reason structural studies of high-index surfaces can be very lengthy originates from the way model reconstructions are proposed, which is based on physical intuition in interpreting scanning tunneling microscope (STM) images. As seen above for the case of Si(5 5 12), the intuitive ways are not very robust for high-index surfaces, since usually more models are required when further experiments are reported. Given the rather large number of low-energy structures that high-index surfaces can have (see, e.g., the case of Si(105)[15, 16]), heuristic approaches pose the risk of

missing the actual physical reconstruction when considering model candidates for comparison with the experimental data. To alleviate this risk, we have recently addressed the reconstruction of semiconductor surfaces as a problem of stochastic optimization [16], and developed two different global search algorithms for the purpose of determining the most favorable surface structure [16, 17]. We have used these global search procedures for studying Si(105) [16, 17] and Si(114) [18], which are both stable orientations for silicon. Although Si(337) is not a stable orientation, its atomic structure can still be pursued with global search algorithms because the only input required is the surface periodicity, which is available from STM [9] and LEED [5] measurements.

In this article we report the results of such a global optimization for the structure and energy of Si(337) using empirical potential and density functional theory calculations. As we shall see, the optimization retrieves most of the previously proposed models [5, 9, 13, 14], as well as a number of other reconstructions that could be relevant for experimental situations where Si(337) nanofacet arises—other than the two (337) unit cells that appear as part of the (5 5 12) structure. The remainder of this paper is organized as follows. In the next section we briefly describe the computational methods used in this study. In Section 3, we present our model structures for the Si(337) surface classified by the number of atoms in the computational cell and their surface energy. In Section 4, we compare our results with other reported Si(337) reconstructions. Our conclusions are summarized in the last section.

## 2 Methods and Computational details

The Si(337) simulation cell consists of two (337) bulk truncated unit cells of dimensions  $a\sqrt{8.375} \times a\sqrt{0.5} \times a\sqrt{67}$ , ( $a$  is the lattice constant of Si), stacked along the  $y$ -direction,  $[\bar{1}10]$ . These dimensions are calculated from the crystal geometry, and are in agreement with the STM images published in Ref. [9], where (337) units are shown as part of a stable reconstructed surface, Si(5 5 12)-(2 × 1).

Because the (337) plane has two-dimensional periodicity along two *non-orthogonal* directions, the rectangular unit in Fig. 1 must be subjected to shifted periodic boundary conditions [19], with the shift in the  $y$ -direction equal to  $a/\sqrt{8}$ . We build a database of structures sorted out by the number of atoms in the simulation cell and by their surface energy calculated with the highly optimized empirical potential developed by Lenosky *et al.* [20]. The number of atoms is varied around the initial value of  $n = 268$ , in order to exhaust all the distinct possibilities that can occur during the search for low energy reconstructions.

The global optimization involved in building the structure database for Si(337) has been performed with the genetic algorithm adapted for crystal surfaces [17]. This algorithm is based on an evolutionary approach in which the members of a generation (pool of models for the surface) evolve with the goal of producing the best specimens, i.e. lowest energy reconstructions. The evolution from one generation to the next takes place by mating, which is achieved by subjecting two randomly picked structures (*parents*) from the pool to an operation that combines their surface features and creates a *child* configuration. This child structure is relaxed and considered for inclusion in the pool, depending on its surface energy. We use two variants of the algorithm, one in which the number of atoms is kept constant for all members of the pool at all times (the constant- $n$  version), and another one in which this restriction is not enforced (the variable- $n$  version). The implementation of this genetic algorithm has recently been described in various degrees of detail in Refs. [17, 18, 21]; for this reason, we will not expand upon it here, but refer the reader to those works. Since the empirical potential may not give a very reliable energy ordering for a database of structures, we study not only the global minima given by HOEP for different values of  $n$ , but also most of the local minima that are within  $15 \text{ meV}/\text{\AA}^2$  from the lowest energy configurations. After creating the set of Si(337) model structures via the genetic algorithm, we recalculate the surface energies of these minima at the level of density functional theory (DFT).

The DFT calculations were performed with the plane-wave based PWscf package [22], using the Perdew-Zunger [23] exchange-correlation energy. The cutoff for the plane-wave energy was set to 12 Ry, and the irreducible Brillouin zone was sampled using 4  $k$ -points. The equilibrium bulk lattice constant was determined to be  $a = 5.41 \text{ \AA}$ , which was used for all the surface calculations in this work. The simulation cell has the single-face slab geometry with a total silicon thickness of  $10 \text{ \AA}$ , and a vacuum thickness of  $12 \text{ \AA}$ . The Si atoms within a  $3 \text{ \AA}$ -thick region at the bottom of the slab are kept fixed in order to simulate the underlying bulk geometry, and the lowest layer is passivated with hydrogen. The remaining Si atoms are allowed to relax until the force components on any atom become smaller than  $0.025 \text{ eV/\AA}$ .

The surface energy  $\gamma$  for each reconstruction is determined indirectly, by first considering the surface energy  $\gamma_0$  of an unrelaxed bulk truncated slab, then by calculating the difference  $\Delta\gamma = \gamma - \gamma_0$  between the surface energy of the actual reconstruction and the surface energy of a bulk truncated slab that has the bottom three layers fixed and hydrogenated. This indirect method for calculating the surface energies at the DFT level was outlined, for instance, in Ref. [24]. The energy of the bulk truncated surface shown in Fig. 1 was found to be  $\gamma_0 = 137.87 \text{ meV/\AA}^2$ . At the end of the genetic algorithm search, we obtain a set of model structures which we sort by the number of atoms in the simulation cell and by their surface energy. These model structures are presented next.

### 3 Results

There are four possibilities in terms of the number of atoms in the slab that yield distinct global energy minima of the Si(337) periodic cell shown in Fig. 1. This has been determined by performing constant- $n$  genetic algorithm optimization for computational slabs with consecutive numbers of atoms  $n$  ( $264 \leq n \leq 272$ ), and identifying a periodic behavior of the lowest surface energy as a function of  $n$ . This procedure of determining the symmetry distinct numbers of atoms in the slab

has been detailed in Ref. [16]. The HOEP global minima, as well as selected local minima of the surface energy for different numbers of atoms are summarized in Table I, along with the density of dangling bonds per unit area and the surface energy computed at the DFT level.

As a general comment, the DFT energy ordering does not coincide with that given by HOEP, indicating that the transferability of HOEP to Si(337) is not as good as in the case of Si(001) and Si(105); to cope with this transferability issue, we have considered more local minima (than listed in Table I) when performing DFT relaxations, as mentioned in Section 2. In the terminology of potential energy surface (PES) theory, we sample the main basins using the genetic algorithm coupled with HOEP, then recalculate the energetic ordering of these basins using DFT. From the table it is apparent that the least favorable number of atoms is  $n = 267$  (modulo 4) at both the HOEP and DFT levels. Therefore, we focus on describing here the reconstructions that have numbers of atoms  $n = 266, 268$ , and  $269$ .

For  $n = 266$  the best model that we obtained at the DFT level is made of a fused assembly of dimers, tetramers and slightly puckered honeycombs, followed (in the  $[7\bar{7}\bar{6}]$  direction) by a row of rebonded atoms. These individual atomic-scale motifs have been reported previously for different surfaces (e.g., [9, 14, 25]), and depicted for convenience in Fig. 2. Their complex assembly shown in Fig. 3(a) has a surface energy of  $94.47 \text{ meV}/\text{\AA}^2$ ; the reconstruction 3(a) has a corrugated aspect when viewed from the  $[\bar{1}10]$  direction, which may account for its relatively high surface energy (refer to Table I). Higher-energy models with  $n = 266$  are illustrated in Fig. 3(b,c,d), and have surface energies ranging from  $2.75 \text{ meV}/\text{\AA}^2$  to about  $7 \text{ meV}/\text{\AA}^2$  above the surface energy of the model 3(a). Dimers (D) and tetramers (T) can be clearly identified on model 3(b), while configuration 3(c) is characterized by the presence of honeycombs (H) and rebonded atoms (R). In model 3(d) the only features from the set in Fig. 2 that can be separately identified are the rebonded atoms R. Nearly degenerate with structure 3(d), we find two other models [3(e) and 3(f), with different tilting of

the dimers belonging to tetramer groups] that contain 6-member ring  $\pi$ -chains [9]. The 6-member rings are labelled by 6-r in Fig. 3(e,f), and are supported by tetramer-like features (denoted by t in Fig. 3) whose dimers are made of fully coordinated atoms.

The optimum number of atoms is  $n = 268$ , as indicated in Table I at both HOEP and DFT levels –coincidentally, this is also the number of atoms that corresponds to two complete (337) bulk truncated primitive cells. We have further verified this number by performing a variable- $n$  genetic algorithm started with all the members in the pool initially having  $n = 267$  atoms. The algorithm has found the correct number of atoms ( $n = 268$ ) and the HOEP global minimum in less than 1000 operations. While different starting configurations may change this rather fast evolution towards the global minimum, our tests indicate that for simulation cells of similar size several thousand genetic operations are sufficient when using the implementation described in Ref. [17]. The lowest energy model as given by DFT is shown in Fig. 4(a) and consists of dimers D, rebonded atoms R and honeycombs H, in this order along  $[77\bar{6}]$ . We note that the number of dangling bonds is smaller at the DFT level (refer to Table I): the reason for the dangling bond reduction is the flattening of the honeycombs (not planar at the level of empirical potentials), which creates two additional bonds with the subsurface atoms. The genetic algorithm search retrieves another low-energy model, in which the dimers are displaced towards and combine with the rebonded atoms, forming tetramers T [Fig. 4(b)]. The two models in Figs. 4(a) and (b) are nearly degenerate, with a surface energy difference of  $\approx 0.5 \text{ meV}/\text{\AA}^2$  relative to one another. A different number and ordering of the structural motifs that are present in Fig. 4(a) gives rise to a noticeably larger surface energy. Specifically, the arrangement of dimers D and honeycombs H [Fig. 4(c)] increases the surface energy by  $4 \text{ meV}/\text{\AA}^2$  relative to the model 4(a). An even higher-energy reconstruction made up of tetramers and rebonded atoms is shown in Fig. 4(d).

When the number of atoms in the simulation cell is  $n = 269$ , we find that the ground state is

characterized by the presence of pentamers, subsurface interstitials, and rebonded atoms [refer to Fig. 5(a)]. Interestingly, this structure is nearly flat, with the rebonded atoms being only slightly out the plane of the pentamers. The pentamers are "supported" by six-coordinated subsurface interstitials. For the Si(337) cell with  $n = 269$  atoms, we find a very strong stabilizing effect of the pentamer-interstitial configuration: the next higher-energy structure [Fig. 5(b)] is characterized by adatoms and rebonded atoms, with a surface energy that is  $\sim 5$  meV/Å<sup>2</sup> higher than that of the ground state in Fig. 5(a). We note that subsurface interstitials have long been reported in the literature to have a stabilizing effect for the reconstruction of Si(113) [24]. Next, we compare the models described above with previously published works on the Si(337) structure.

## 4 Discussion

To our knowledge, the first model of the Si(337) surface was proposed by Baski, Erwin and Whitman in their original work on the structure of Si(5 5 12) [9]. The model contained surface tetramers and 6-member ring  $\pi$ -chains, and was similar to the structures depicted in Fig. 3(e,f). We observed a strong relaxation of the  $\pi$ -bonded chain, in which one of the atoms of each 6-ring protrudes out of the surface and settles well-above its neighbors. The surface energy of the model 3(f) is not particularly favorable, although it is the lowest of all the models containing 6-ring  $\pi$ -chains that we have investigated. Heuristically speaking, if the under-coordinated atoms of the 6-rings are removed (4 atoms per  $(2 \times 1)$  unit cell), then one would obtain the model of Hu *et al.* [5], which is made of dimers and tetramers. The genetic algorithm with  $n = 266$  (modulo 4) has also retrieved this model, which is shown in Fig. 3(b) after DFT relaxation.

Models 3(b,e,f) have a high density of dangling bonds (db) per unit area,  $10\text{db}/a^2\sqrt{16.75}$ . While the dangling bond density may seem to account for the large surface energy of these models, a close inspection of Table I shows that, in fact, there is no clear correlation between the dangling bonds

and the surface energy. For instance, at the same number of unsaturated bonds per area, models 3(b,e,f) span a  $4 \text{ meV}/\text{\AA}^2$  range in surface energy. Furthermore, if we take the DFT model 3(a) as reference, we note that an increase by one db per unit cell [from 3(a) to 3(c)] results in a surface energy increase of  $\approx 7 \text{ meV}/\text{\AA}^2$ ; on other hand, an increase of seven db in the simulation cell [from 3(a) to 3(b)] increases the surface energy by less than  $3 \text{ meV}/\text{\AA}^2$ . Similar arguments for the lack of correlation between missing bonds and surface energy can be made by analyzing structures with other numbers of atoms in Table I. At the optimum number of atoms ( $n = 268$ ), we find that with the same dangling bond density, models 4(a,b,c) span a  $4 \text{ meV}/\text{\AA}^2$  surface energy range: this range is so large that it includes the global minimum as well as higher surface energy local minima that may not be observable in usual experiments. These findings are consistent with the statement that the minimization of surface energy is not controlled solely by the reduction of the dangling bond density, but also by the amount of surface stress caused in the process [9]. Given that the heuristic approaches may only account for the dangling bond density when proposing candidate reconstructions, the need for robust minimization procedures (e.g., [16, 17]) becomes apparent.

A notable configuration with  $4\text{db}/a^2\sqrt{16.75}$  is shown in Fig. 3(c), where the bonds that join the (lower corner of) honeycombs and the neighbors of the rebonded atoms are markedly stretched beyond their bulk value. The stretched bonds [indicated by arrows in Fig. 3(c)] cause the surface energy to become very high,  $100.39 \text{ meV}/\text{\AA}^2$  at the DFT level. Interestingly, the surface stress (and surface energy) is very efficiently lowered by adding dimers such that stretched bonds in 3(c) are broken, and the dimers "bridge" over as shown in Fig. 4(a). The addition of one dimer per simulation cell results in the most stable Si(337) reconstruction that we found, with  $\gamma \approx 89 \text{ meV}/\text{\AA}^2$ . A structure similar to 4(a) was previously proposed by Liu and coworkers [13] to explain their HRTEM data. These authors also proposed a possible configuration for the other unit of (337) that is part of the large Si(5 5 12) unit cell, which has essentially the same bonding topology as 4(b).

Although no atomic scale calculations were performed in Ref. [13], the two (337) models of Liu *et al.* were in qualitative agreement with more recent DFT results by Jeong *et al.* [14], as well as with STM and HRTEM images. When performing ab-initio relaxations, we found that the HOEP models that corresponded most closely to those in Ref. [13] end up relaxing into the configurations put forth by Jeong and coworkers [14]. The structures shown in Fig. 4(a,b) allow for (337) nanofacets to intersect (113) facets without any bond breaking or rebonding. This absence of facet-edge rebonding, as well as the relatively low energy of Si(337), give rise to short-range attractive interactions between steps on miscut Si(113) [26], which is consistent with the experimental observation of (337) step-bunched phases [11].

## 5 Conclusions

In summary, we have presented an investigation of the Si(337)-(2 × 1) reconstructions based on a genetic algorithm search for the most favorable atomic configuration [17, 21]. We have coupled the algorithm with the HOEP model [20] for atomic interactions in order to efficiently create a database of Si(337) models. Since no empirical interatomic potential can be expected to be fully transferable to arbitrary surface orientations, we have relaxed the database reconstructions using ab initio DFT calculations. The DFT relaxations give a more accurate idea about the relative stability of the reconstructions found, and help identify the likely lowest-energy candidates that are shown in Fig. 4(a) and (b). As it turns out, the two models coincide with those proposed by Jeong and coworkers [14] from STM experiments and density functional calculations. This finding lends strong support to the minimization approach taken here and shows that sampling the configuration space using the HOEP potential [20] is a versatile way to find good candidate reconstructions for high-index Si surfaces. We hope that the development of algorithms for surface structure determination [16, 17] would also stimulate further research towards interatomic potentials

with improved transferability, since the use of such potentials will improve the quality of the model structures found during the global optimization: in turn, this would increase the range of materials problems where the search algorithms can be used to gain knowledge of optimal structure.

The DFT surface energies of the (337) models shown in Fig. 4(a,b) are relatively small, being about  $1 \text{ meV}/\text{\AA}^2$  higher than the surface energy of Si(114) computed using the same computational parameters Section 2. Upon analyzing the results of the genetic algorithm optimization, we have seen that the (337) structures with low surface energies correspond to certain spatial arrangements of atomic-scale motifs (Fig. 2), rather than to a minimum number of dangling bonds per unit cell. In experiments, particular conditions can readily appear such as to favor the stabilization of Si(337) over Si(5 5 12), as shown for instance in Refs. [3, 4]. Recent works by Baski and coworkers [27] reveal a controlled way in which Si(337) facets can be formed –the deposition of gold. At Au coverages of 0.15 ML, the (5 5 12) orientation facets into Si(113) and Si(337), with the (337) surface unit cells being twice as large as the ones in Fig. 1 along the  $[\overline{776}]$  direction. Since the Au coverages at which Si(337) emerges correspond to only a couple of Au atoms per each (337) unit, the models presented here can be used as building blocks for the structure of Si(337)-Au nanofacets observed in [27], as well as in other experimental situations.

**Acknowledgments.** CVC thanks J. Dabrowski, S.C. Erwin, S. Jeong, and M. Takeguchi for correspondence on their model reconstructions [24, 9, 14, 13]. Ames Laboratory is operated for the U.S. Department of Energy by Iowa State University under Contract No. W-7405-Eng-82; this work was supported by the Director of Energy Research, Office of Basic Energy Sciences. We gratefully acknowledge grants of supercomputer time from EMSL at Pacific Northwest National Laboratory, from NCSA (DMR-050031N), and from NERSC.

## References

- [1] Z. Gai, R.G. Zhao, W.J. Li, Y. Fujikawa, T. Sakurai, and W. S. Yang, Phys. Rev. B **64**, 125201 (2001).
- [2] A.A. Baski, S.C. Erwin, and L.J. Whitman, Surf. Sci. **392**, 69 (1997).
- [3] W. Ranke and Y.R. Xing, Phys. Rev. B **31**, 2246 (1985).
- [4] J.G.E. Gardeniers, W.E.J.R. Maas, R.Z.C. van Meerten, and L.J. Giling, J. Cryst. Growth **96**, 821(1989).
- [5] X.M. Hu, E.G. Wang, and Y.R. Xing, Appl. Surf. Sci. **103**, 217 (1996).
- [6] A.A. Baski and L.J. Whitman, Phys. Rev. Lett. **74**, 956 (1995).
- [7] A.A. Baski and L.J. Whitman, J. Vac. Sci. Technol. A **13** 1469 (1995).
- [8] A.A. Baski and L.J. Whitman, J. Vac. Sci. Technol. B **14**, 992 (1996).
- [9] A.A. Baski, S.C. Erwin, and L.J. Whitman, Science **269**, 1556 (1995).
- [10] S. Song, M. Yoon, and S.G.J. Mochrie, Surf. Sci. **334**, 153 (1995).
- [11] M. Takeguchi, Y. Wu, and K. Furuya, Surf. Interf. Anal. **30**, 288 (2000).
- [12] W. Ranke and Y.R. Xing, Surf. Rev. Lett. **4**, 15 (1997).
- [13] J. Liu, M. Takeguchi, H. Yasuda, and K. Furuya, J. Cryst. Growth, **237**, 188 (2002).
- [14] S. Jeong, H. Jeong, S. Cho, and J. M. Seo, Surf. Sci. **557**, 183 (2004).
- [15] C.V. Ciobanu, V.B. Shenoy, C.Z. Wang, and K.M. Ho, Surf. Sci. **544**, L715 (2003).
- [16] C.V. Ciobanu and C. Predescu, Phys. Rev. B **70**, 085321 (2004).

- [17] F.C. Chuang, C.V. Ciobanu, V.B. Shenoy, C.Z. Wang, and K.M. Ho, Surf. Sci. **573**, L375 (2004).
- [18] F.C. Chuang, C.V. Ciobanu, C. Predescu, C.Z. Wang, and K.M. Ho, Surf. Sci. **578**, 183 (2005).
- [19] T.W. Poon, S. Yip, P.S. Ho, and F.F. Abraham, Phys. Rev. B **45**, 3521 (1992).
- [20] T.J. Lenosky, B. Sadigh, E. Alonso, V.V. Bulatov, T. Diaz de la Rubia, J. Kim, A.F. Voter, and J.D. Kress, Modelling Simul. Mater. Sci. Eng. **8**, 825 (2000).
- [21] H.J.W. Zandvliet, Surf. Sci. **577**, 93 (2005).
- [22] S. Baroni, A. Dal Corso, S. de Gironcoli, and P. Giannozzi, <<http://www.pwscf.org>>.
- [23] J.P. Perdew and A. Zunger, Phys. Rev. B **23**, 5048 (1981)
- [24] J. Dabrowski, H.J. Müssig, G. Wolff, Phys. Rev. Lett. **73**, 1660 (1994).
- [25] S.C. Erwin, A.A. Baski, and L.J. Whitman, Phys. Rev. Lett. **77**, 687 (1996).
- [26] C.V. Ciobanu, D.T. Tambe, V.B. Shenoy, C.Z. Wang, and K.M. Ho, Phys. Rev. B **68**, 201302 (2003).
- [27] A.A. Baski and K.M. Saoud, J. Cluster Sci. **12**, 527 (2001); J.W. Dickinson, J.C. Moore and A.A. Baski, Surf. Sci. **561**, 193 (2004).



Table I: Surface energies of selected Si(337)-(2×1) reconstructions, sorted by the number of atoms  $n$  in the periodic cell. The second column shows the number of dangling bonds per unit area, counted after relaxation with HOEP; the dangling bond density at the DFT level is shown in parentheses. Columns three and four list the surface energies given by the HOEP potential [20] and by density functional calculations [22].

| $n$ | Bond counting<br>(db/ $a^2\sqrt{16.75}$ ) | HOEP<br>(meV/Å <sup>2</sup> ) | DFT<br>(meV/Å <sup>2</sup> ) | Fig. |
|-----|---|-------------------------------|------------------------------|------|
| 266 | 10 (10)                                   | 87.37                         | 109.04                       |      |
|     | 10 (10)                                   | 87.74                         | 97.22                        | 3(b) |
|     | 6 (4)                                     | 87.79                         | 100.39                       | 3(c) |
|     | 10 (10)                                   | 89.60                         | 102.35                       |      |
|     | 10 (10)                                   | 89.79                         | 101.58                       | 3(e) |
|     | (10)                                      | —                             | 101.16                       | 3(f) |
|     | 4 (3)                                     | 92.07                         | 94.47                        | 3(a) |
|     | 4 (4)                                     | 93.87                         | 101.43                       | 3(d) |
| 267 | 8 (8)                                     | 92.35                         | 99.95                        |      |
|     | 8 (8)                                     | 92.37                         | 96.47                        |      |
|     | 10 (8)                                    | 92.47                         | 107.72                       |      |
|     | 9 (8)                                     | 99.11                         | 101.33                       |      |
| 268 | 8 (6)                                     | 81.99                         | 93.13                        | 4(c) |
|     | 8 (8)                                     | 83.11                         | 95.17                        |      |
|     | 8 (6)                                     | 83.43                         | 89.61                        | 4(b) |
|     | 8 (8)                                     | 84.90                         | 94.52                        | 4(d) |
|     | 8 (6)                                     | 85.47                         | 90.19                        |      |
|     | 8 (6)                                     | 85.94                         | 89.12                        | 4(a) |
| 269 | 4 (4)                                     | 89.18                         | 93.50                        | 5(a) |
|     | 6 (6)                                     | 92.58                         | 99.21                        | 5(b) |

**Figure Captions. All figures COLOR ONLINE ONLY**

Fig. 1. Top and side view of the unreconstructed Si(337) surface. The rectangle represents the simulation cell that is subjected to shifted periodic boundary conditions [19], and the solid arrows are the corresponding periodic vectors; four such periodic cells are shown in the figure in order to aid the eye with the shifted boundary conditions. The darker shade marks the undercoordinated surface atoms.

Fig. 2. Structural features (top and side views) that can be present on low-energy Si(337) reconstructions: (a) dimers, (b) rebonded atoms, (c) tetramers, and (d) honeycombs. In each case, the atoms that make up the motif are shown in darker shade.

Fig. 3. Models of Si(337) reconstructions with  $n = 266$  atoms per  $(2 \times 1)$  unit cell, after DFT relaxation (top and side views). The surface energy computed from first-principles is indicated for each structure, along with the corresponding value (in parentheses) determined with the HOEP interaction model [20]. The dark shade marks the undercoordinated atoms. The four-coordinated atoms that are exposed at the surface are shown in white. Apart from the relaxations, dimer tilting, and perhaps the relative phase of dimerization, the structure shown in panel (b) is the same as that proposed in Ref. [5], and reconstructions in panels (e) and (f) are similar to the model in Ref. [9].

Fig. 4. Si(337) reconstructions with  $n = 268$  atoms per  $(2 \times 1)$  unit cell, after DFT relaxation (top and side views). The surface energy computed from first-principles is indicated for each structure, along with the corresponding value (in parentheses) determined with the HOEP interaction model [20]. The dark shade marks the undercoordinated atoms, while the four-coordinated atoms that are exposed at the surface are shown in white. The lowest-energy Si(337)- $(2 \times 1)$  reconstruc-

tions are shown in panels (a) and (b). These structures differ in the position of the dimers in the unit cell: the dimers D can be part of a 7-member ring [side view, panel (a)], or be part of a tetramer T [panel (b)]. The models shown in panels (a) and (b) are the same as those reported in Ref. [14] for the two (337) units that are part of a (5 5 12) cell.

Fig. 5. Models of Si(337) reconstructions with  $n = 269$  atoms per  $(2 \times 1)$  unit cell, after DFT relaxation (top and side views). The surface energy computed from first-principles is indicated for each structure, along with the corresponding value (in parentheses) determined with the HOEP interaction model [20]. The dark blue marks the undercoordinated atoms, while the four-coordinated atoms that are exposed at the surface are shown in white. The best  $n = 269$  model [panel(a)], is stabilized by flat pentamers and subsurface interstitials.

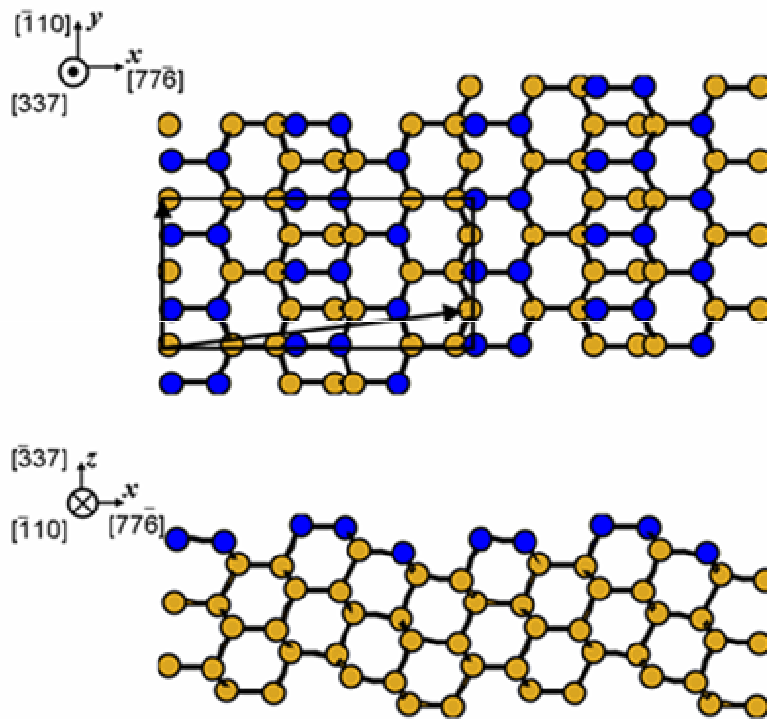


Figure 1: COLOR ONLINE ONLY. Chuang, Ciobanu, Wang, Ho

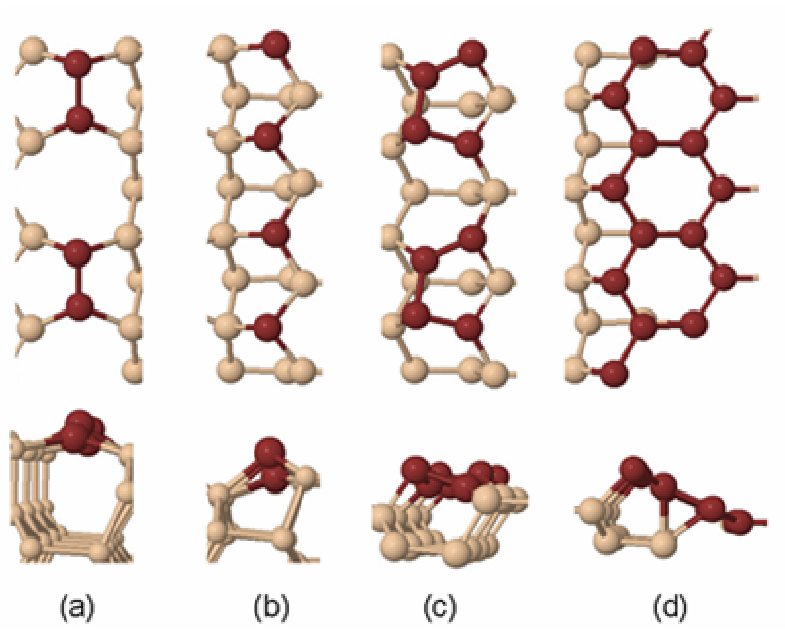


Figure 2: COLOR ONLINE ONLY. Chuang, Ciobanu, Wang, Ho

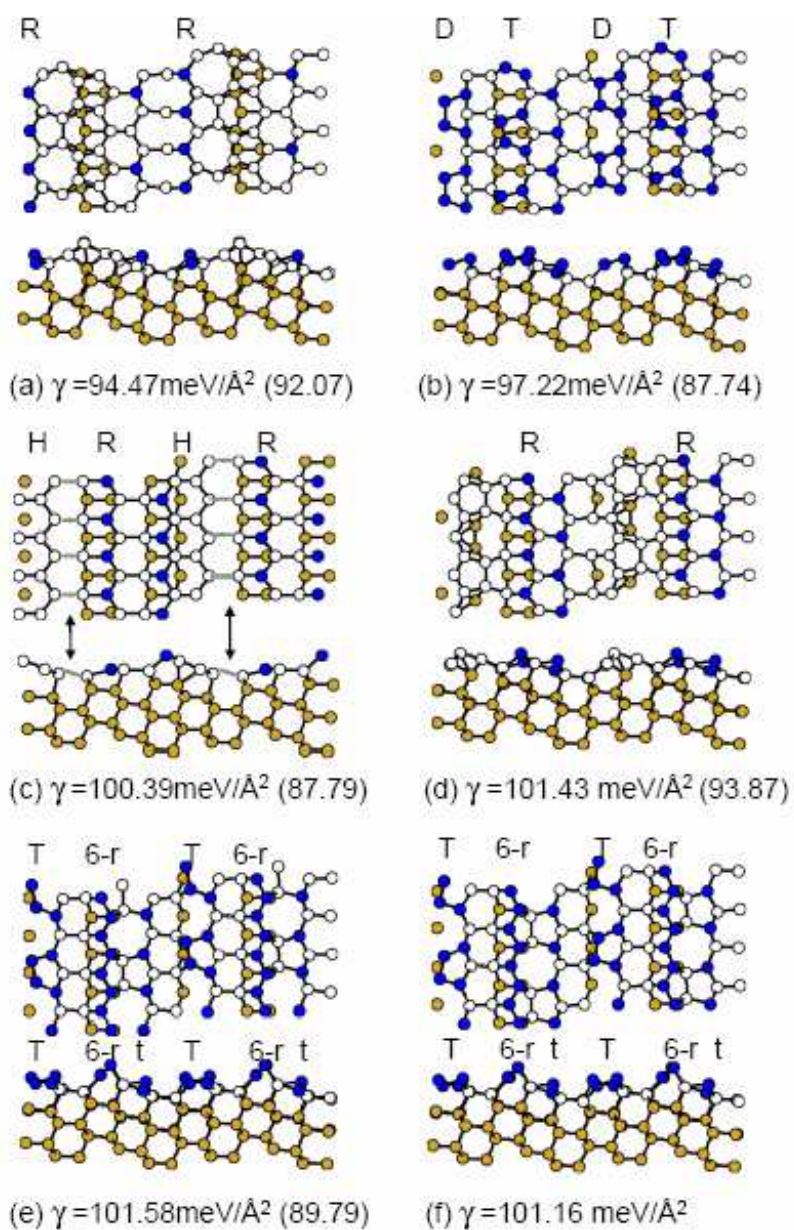


Figure 3: COLOR ONLINE ONLY. Chuang, Ciobanu, Wang, Ho

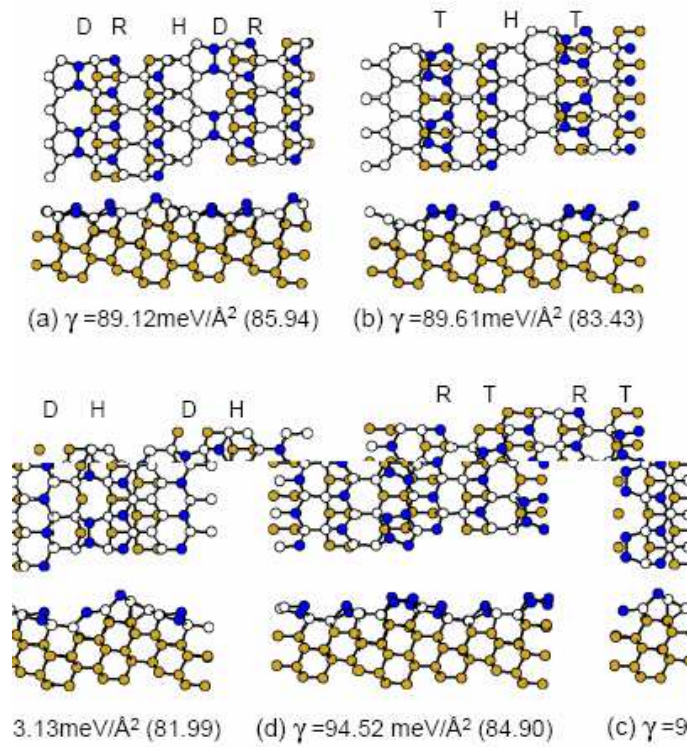


Figure 4: COLOR ONLINE ONLY. Chuang, Ciobanu, Wang, Ho

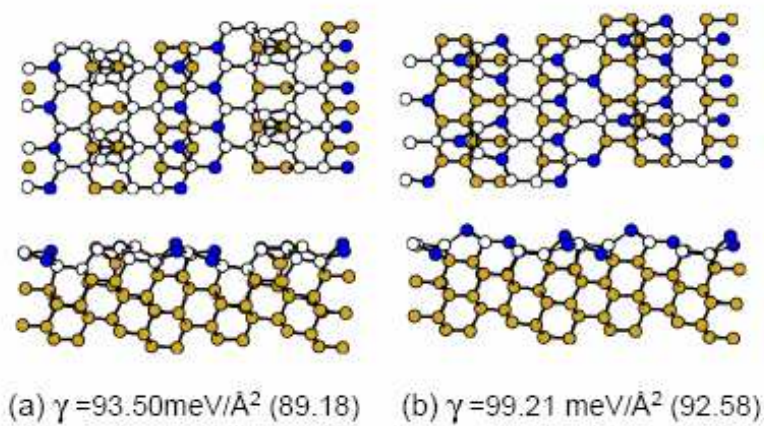


Figure 5: COLOR ONLINE ONLY. **Chuang, Ciobanu, Wang, Ho**